

Segmentation of nearly isotropic overlapped tracks in photomicrographs using successive erosions as watershed markers

Alexandre Fioravante de Siqueira^{a,b,*}, Wagner Massayuki Nakasuga^a, Sandro Guedes^a, Raymond Jonckheere^b, Lothar Ratschbacher^b

^a*Departamento de Raios C3smicos e Cronologia, IFGW, University of Campinas*

^b*Institut f3ur Geologie, TU Bergakademie Freiberg*

Abstract

The major challenges of automatic track counting are distinguishing tracks and material defects, identifying small tracks and defects of similar size, and detecting overlapping tracks. Here we address the latter issue using WUSEM, an algorithm which combines the watershed transform, morphological erosions and labeling to separate regions in photomicrographs. WUSEM shows reliable results when used in photomicrographs presenting almost isotropic objects. We tested this method in two datasets of diallyl phthalate (DAP) photomicrographs and compared the results with manual counting. The automatic/manual efficiency ratio is higher than 0.87 for both datasets.

Keywords: Automatic counting, Diallyl phthalate, Digital image processing, Fission track dating

1. Introduction

The fission track dating (FTD) is based on the spontaneous fission of ^{238}U , an impurity in natural minerals such as apatite and zircon [1]. The fission process releases two fragments that trigger the displacement of atoms, leading to a net

*Corresponding author. Phone: +55(19)3521-5362.

Email addresses: siqueiraaf@gmail.com (Alexandre Fioravante de Siqueira), wamassa@gmail.com (Wagner Massayuki Nakasuga), sguedes@ifi.unicamp.br (Sandro Guedes), jonckhee@geo.tu-freiberg.de (Raymond Jonckheere), lothar.ratschbacher@geo.tu-freiberg.de (Lothar Ratschbacher)

structural modification called latent track. After a convenient etching process, channels are formed along the latent track trajectory and become visible under an optical microscope.

The external detector method (EDM), where spontaneous tracks are counted in the mineral and induced fission tracks are counted in the external detector, is commonly used for FTD. Muscovite mica is the most used external detector, but diallyl phthalate (DAP) has been proposed as an alternative: DAP is uranium-free, etching for track revelation is less corrosive, and tracks are isotropically etched [2, 3, 4, 5], which makes tracks in DAP suitable for automatic counting.

Track counting is usually performed with an optical microscope. Photomicrographs can also be used, which could improve the counting accuracy [6]. Procedures for measuring and counting tracks are time-consuming and involve practical problems, e.g. variation in observer efficiency [7]. An automatic method based on image processing techniques could increase the track counting rate and improve counting reproducibility. However, separating elements in nontrivial images is one of the hardest tasks in image processing [8].

Automatic systems for separating, counting or measuring tracks have been studied for a while, and several solutions were presented (e.g. [9, 10, 11, 12, 13, 14, 15, 16, 17, 18, 19, 20, 21, 22, 23, 7, 24, 25]). Still, the precision of automatic methods is not satisfactory yet; an automatic analysis could need to be manually adjusted by the operator, being more time consuming than the usual measure [22, 26]. The major challenges to automatic track counting are detecting overlapping tracks, distinguishing tracks and material defects (e.g. surface scratches due to polishing), and identifying small tracks and defects of comparable size in the background of photomicrographs [7].

To address the problem of identifying overlapping ion tracks in photomicrographs, we propose an algorithm based on the watershed transform [27] using morphological erosions [28] as markers. A similar method was used to separate packings of ellipsoidal particles represented using X-Ray tomography [29]. We tested this method in two datasets of diallyl phthalate (DAP) photomicrographs, and used the results to relate the incident track energy with the mean

gray levels and mean diameter products for each sample from the first dataset. Applications such as radon monitoring and neutron dosimetry in boron neutron capture therapy (BNCT, e.g. [30]) could benefit from this approach: in BNCT, the PADC detector is used to detect alpha particles, protons, and lighter ions, and tracks in PADC are similar to those in DAP.

2. Material and methods

2.1. Watershed Using Successive Erosions as Markers (WUSEM) algorithm

Here we present the WUSEM (Watershed Using Successive Erosions as Markers) algorithm, which combines morphological erosions [28], the watershed transform [27] and labeling [31] algorithms to separate regions of interest (ROI) in binary images. To exemplify WUSEM's capabilities, it is used to separate overlapping tracks within the test photomicrographs (Figure 1).

The WUSEM algorithm follows:

1. The user define an initial radius (r_0) and an iterative radius (Δr) to a structuring element (Figure 2).
2. The input binary image is eroded using the structuring element with radius equal to r_0 . This erosion is used as a marker to the watershed algorithm. Then, the resulting image is labeled. This is the first iteration.
3. A new structuring element is defined. Its radius is $r_0 + \Delta r$. The input binary image is eroded with this new structuring element, the erosion is used as a marker to watershed, and the result is labeled. This is the second iteration.
4. The process continues until the eroded image does not have objects. Then, all iterations are summed and the result is labeled again, to reorder the ROI.

WUSEM is implemented in the function `segmentation_wusem()`, available in the Supplementary Material. It receives the arguments `str_el`, `initial_radius` and `delta_radius`, representing the structuring elements, r_0 and Δr , respectively.

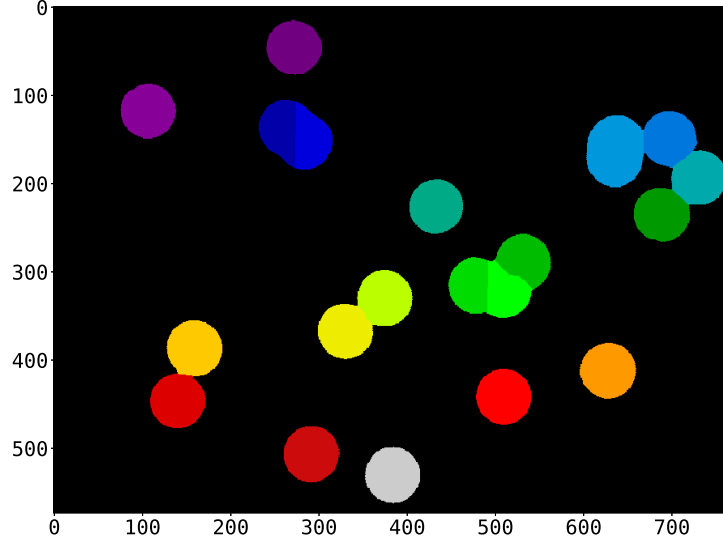


Figure 1: WUSEM algorithm application in an input image. First, the image is binarized using the ISODATA threshold. Then, the image is eroded using initial radius (r_0) and iterative radius (Δr) equal to 1 and 1 respectively, to ease visualization. The process continues until the eroded image has regions in it. All erosions are summed, and the result is labeled; each labeled track receives a color from the `nipy_spectral` colormap. Finally, the function `enumerate_objects()` is used to number the found tracks. Final results are shown to r_0 and Δr equal to 25 and 2, respectively. Animation also available at <https://youtu.be/gYKbqME0hB0>.

2.2. DAP photomicrographs

We used two sets of diallyl phthalate (DAP, $C_{14}H_{14}O_4$) photomicrographs to test the WUSEM algorithm. One of them was obtained from detectors irradiated with ^{78}Kr tracks, and the other has induced fission tracks.

2.2.1. ^{78}Kr tracks

The first dataset contains 400 photomicrographs of tracks from nine different DAP plaques irradiated with ^{78}Kr ions at a nominal fluence of $1.4 \times 10^5 cm^{-2}$, from a beam perpendicular to the detector surfaces at GSI, Darmstadt, Germany.

During the irradiation, detectors were covered with aluminum foils forming a moderation layers of thicknesses varying from zero (no cover) to $90 \mu m$. De-

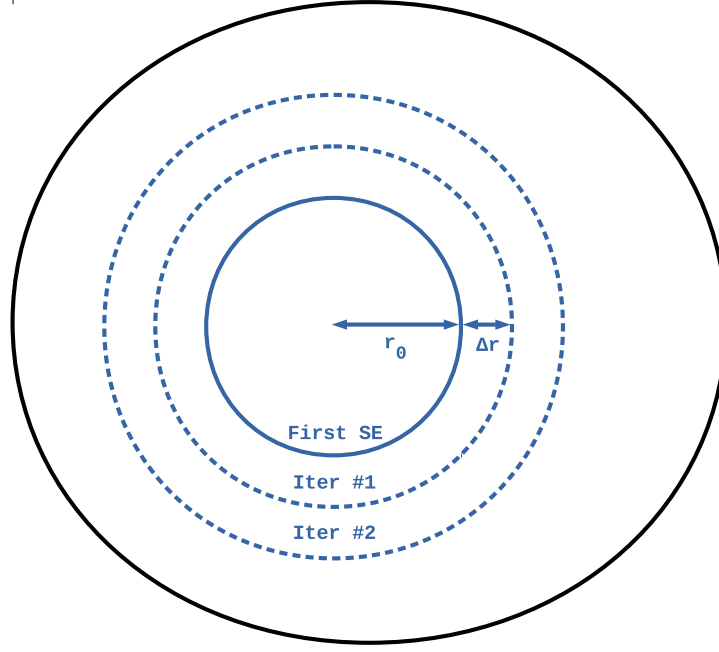


Figure 2: Representation of structuring elements defined for each iteration of the WUSEM algorithm for an interest region. The radius of the first, second and third structuring elements are r_0 , $r_0 + \Delta r$ and $r_0 + 2\Delta r$, respectively.

tectors were named after their cover thicknesses (K0, K20, K30, ..., K90). Ions arrived at the setup with initial energy of 865 MeV and were slowed down in the aluminum cover before hitting the detector surface. Incidence energies were calculated using the software SRIM [32], and varied from 18 MeV ($90 \mu m$ cover) to 865 MeV (no cover). Detectors were etched in a PEW solution (7.5 g KOH, 32.5 g ethanol, 10 g water) solution for 4.5 ± 0.2 min at $65 \pm 3^\circ C$.

Images were captured with a CCD camera coupled with a Zeiss microscope, in reflected light mode, under $1250 \times$ nominal magnification. Then, the detectors were further etched for 4 minutes, total of 8.5 ± 0.3 min, and new images were captured. This way, we obtained 18 subsets of images. Tracks within these photomicrographs are almost isotropic and have the same orientation, resembling circles.

2.2.2. Induced fission tracks

The second dataset contains 19 photomicrographs with two different magnifications from a DAP plaque used as external detector, coupled to an apatite sample and irradiated with thermal neutrons to induce fission in the ^{235}U atoms inside the mineral. During the fission process, two fragments are released and, eventually, are detected by the DAP plaque. Fragments arrive at the detector surface with different energies and incidence angles, resulting in a variety of track formats. Hence, counting tracks in these photomicrographs is more complex than in the previous case.

2.3. License and reusability

The WUSEM algorithm and several functions for its implementation lie within the packages Numpy [33], Scipy [34], Matplotlib [35], scikit-image [36], among others. All code published with this paper is written in Python 3 [37] and is available under the GNU GPL v3.0 license, and all photomicrographs and figures distributed with this paper are available under the CC-BY 2.0 license.

3. Experimental

3.1. Processing photomicrographs of ^{78}Kr tracks

3.1.1. Exemplifying the methodology

Here we use a photomicrograph from the first dataset¹ (Figure 3) to exemplify the WUSEM method. We binarized this photomicrograph using the ISODATA threshold [38, 39]; then, the WUSEM algorithm separates the overlapping tracks.

Binary images were generated according to two scenarios (Figure 4):

- Maintaining regions connected to the image border. We refer to this scenario as “*considering border tracks*” throughout the text. The manual

¹First image from the folder `orig_figures/dataset.01/Kr-78.4,5min/K90_incid`. Available in the Supplementary Material.

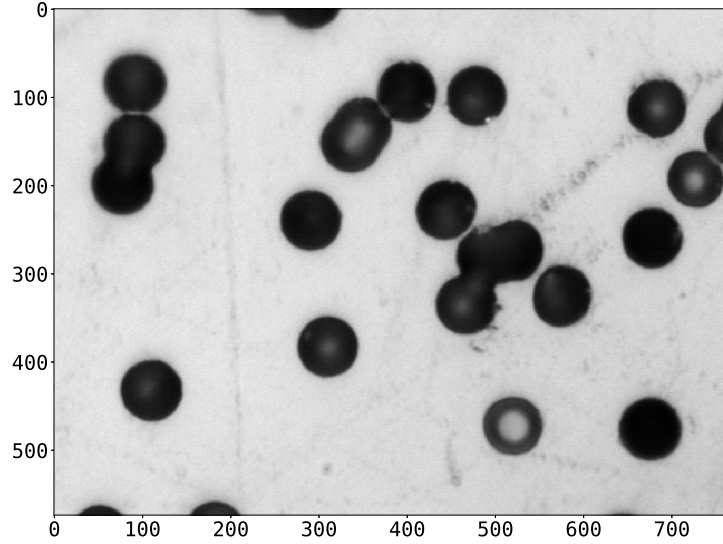


Figure 3: Photomicrograph from the first dataset, presenting tracks in a DAP sample. Colormap: `gray`.

counting criteria for this scenario was to count all tracks that appear in the photomicrograph.

- Removing regions connected to the image border, using the function `segmentation.clear_border()` from `scikit-image`. We refer to this scenario as “*ignoring border tracks*” throughout the text. The manual counting criteria for this scenario was to count a track when the observer judges that it is entirely inside the photomicrograph.

Different gray levels in some tracks may not be properly separated, complicating the extraction of track features. To address this issue, we filled the regions in the binary image using the function `ndimage.morphology.binary_fill_holes()` from `scipy`. Then, the WUSEM algorithm is applied. For this example, we chose `initial_radius = 5` and `delta_radius = 2` as parameters. WUSEM returns a labeled region, which can be used as parameter to the function `enumerate_objects()` (Figure 5).

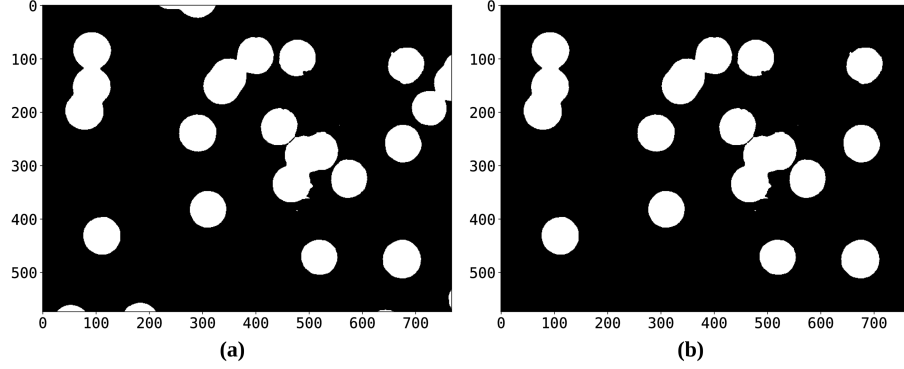


Figure 4: Input photomicrograph binarized using the ISODATA threshold (threshold = 128) and region filling. (a) Considering border tracks. (b) Ignoring border tracks. Colormap: **gray**. Note that tracks connected to the border tracks are also removed by the algorithm, while they would be counted by the observer.

3.1.2. Comparison between manual and automatic counting

An experienced observer can easily distinguish tracks in the photomicrograph, even when several tracks are superimposed. For this reason, manual counting is considered the control in the comparison with the automatic counting. In the following, the WUSEM algorithm is applied to the photomicrograph set and the processing parameters are studied.

We established an arbitrary value of up to 2.5 tracks less than the mean of the manual counting as a tolerance. WUSEM’s parameters become candidates if the automatic counting lies within the tolerance interval, i.e. $0 < \mu_{n_{\text{manual}}} - n_{\text{auto}} < 2.5$, where n is the track number obtained by each approach (Figure 6).

WUSEM’s best parameters for this study are the ones within the tolerance interval for most samples. According to the stated comparison, the best parameters are `initial_radius` = 5 and `delta_radius` = 4 when considering border tracks, and `initial_radius` = 25 and `delta_radius` = 2 when ignoring border tracks. Using the best parameters defined, we compared manual and automatic counting for each sample (Figure 7, Tables 1 and 2).

Since tracks in this dataset have the same shapes, we can attribute an efficiency of 100 % for manual counting. Automatic counting was initially set

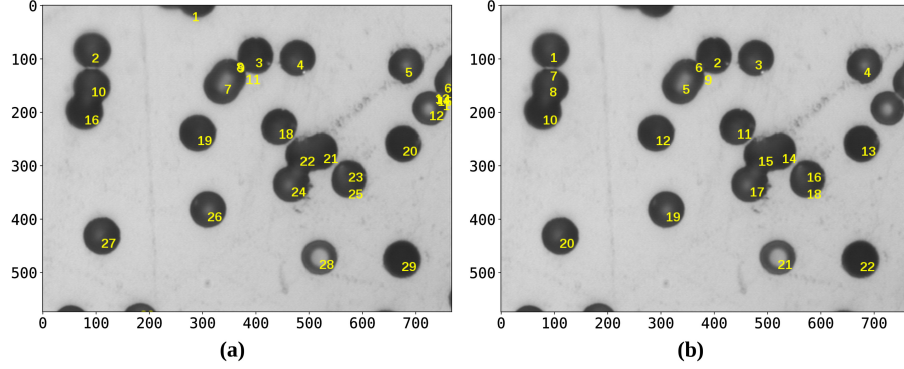


Figure 5: Tracks separated in Figure 3 using the WUSEM algorithm and enumerated using `enumerate_objects()`. Since the size of the first structuring element is small when compared to the objects, smaller regions where tracks overlap are counted as tracks, e.g.: (a) 7, 8, 9, and 11 (only two tracks). (a) Considering border tracks. (b) Ignoring border tracks. Parameters for WUSEM algorithm: `initial_radius = 5`, `delta_radius = 2`.

to obtain a smaller number of tracks when compared to the manual counting. However, the automatic counting returns false positives, i.e., incorrectly labels background regions as ROI (points above the 1:1 line in Figures 7 (b) and (d)). To avoid false positives, one could use a more restrictive criterion than the presented here.

Sample	Manual counting ($\mu \pm \sigma$)		Automatic counting ($\mu \pm \sigma$)		Efficiency $\pm \sigma$	
	4.5 min	8.5 min	4.5 min	8.5 min	4.5 min	8.5 min
K0	24 \pm 4	23 \pm 3	22 \pm 3	22 \pm 3	0.93 \pm 0.08	0.96 \pm 0.09
K20	29 \pm 5	27 \pm 5	27 \pm 5	25 \pm 4	0.93 \pm 0.11	0.95 \pm 0.13
K30	27 \pm 4	28 \pm 4	26 \pm 4	28 \pm 6	0.95 \pm 0.07	0.99 \pm 0.10
K40	27 \pm 4	27 \pm 6	26 \pm 3	26 \pm 6	0.96 \pm 0.10	0.98 \pm 0.11
K50	28 \pm 3	26 \pm 5	26 \pm 4	23 \pm 4	0.94 \pm 0.12	0.90 \pm 0.09
K60	30 \pm 4	28 \pm 5	30 \pm 5	27 \pm 6	0.99 \pm 0.07	0.96 \pm 0.12
K70	23 \pm 4	21 \pm 5	22 \pm 4	20 \pm 6	0.97 \pm 0.09	0.97 \pm 0.11
K80	24 \pm 4	24 \pm 6	23 \pm 4	23 \pm 5	0.97 \pm 0.09	0.98 \pm 0.14
K90	28 \pm 4	25 \pm 4	29 \pm 6	27 \pm 6	1.02 \pm 0.10	1.05 \pm 0.12

Table 1: Mean, standard deviation, and automatic/manual efficiency ratio for for each sample of the first dataset, when considering border tracks.

Counting reproducibility is important for considering the reliability of track

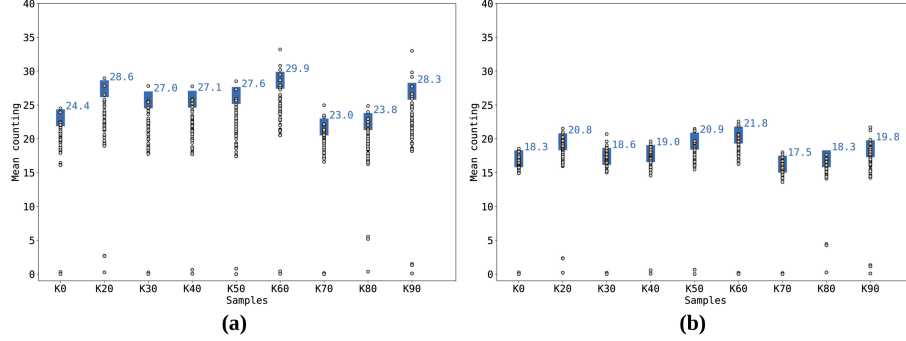


Figure 6: Manual counting mean (top of the blue bar; values on the right) for each sample and automatic counting results with mean within (orange points) and outside (gray points) the tolerance interval (blue bar) for the second dataset. (a) Considering borders. (b) Ignoring borders.

counting. Despite the variations in track characteristics, the efficiencies of WUSEM’s automatic counting remained constant within uncertainties, when compared to manual counting. Results are very similar for tracks of the two etching conditions, whether considering or ignoring border tracks.

3.1.3. Relating ion energies with diameter product and mean gray levels

In this application, we use WUSEM to relate the track energies to the product of major and minor diameters ($D_>$ and $D_<$, respectively) and the mean gray level for each track. The algorithm seems to introduce regions with small areas in the images. To ensure reliability in the next steps, we used regions with $D_<$ within the interval $\mu \pm 3\sigma$ (Figure 8), excluding regions that are too small to be tracks.

We considered only approximately circular tracks in our analysis, based on an eccentricity (ϵ)² criterion: ϵ should be equal to or less than 0.3 (Figure 9). Then, after tracks were fully separated, we could measure their gray levels and diameters. This additional criterion could have been carried out also for count-

²In image processing, the eccentricity of an object is a number in the interval $[0, 1)$. The lower the value, the region becomes closer to a circle.

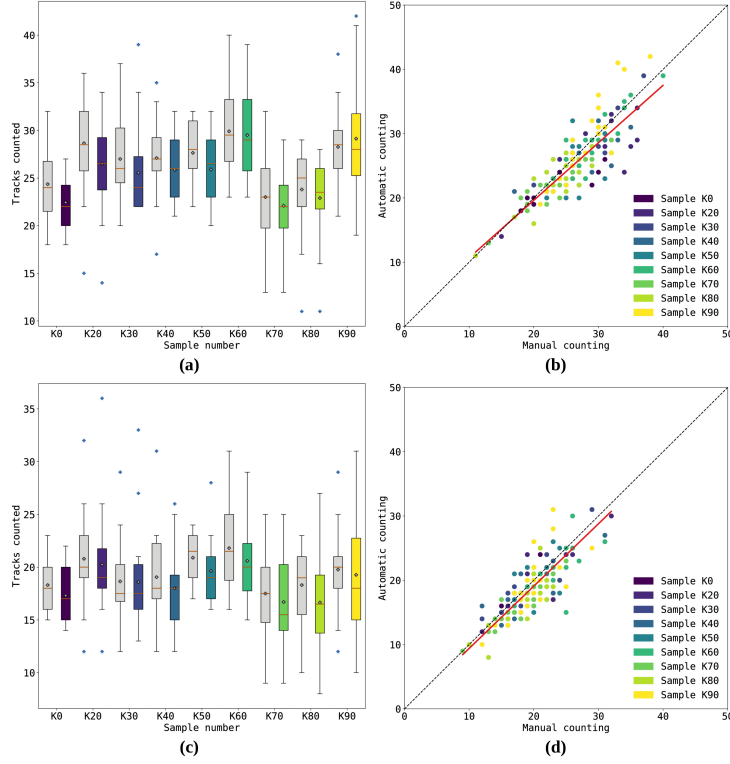


Figure 7: Comparison between manual and automatic counting for 4.5 min etching samples, when (a, b) considering border tracks and (c, d) ignoring border tracks. Compared to manual counting, automatic results variate less when ignoring borders. (a, c) gray: manual counting. Red line: distribution median. White signal: distribution mean. (b, d) dashed: 1:1 line. Red line: regression for the experimental data.

ing tracks, to ensure that false positives (spurious objects counted as tracks) are avoided.

After separating each track, we can obtain their gray levels and diameters. Once the mean gray level and diameters of each track in a photomicrograph are obtained, we can relate them with the incident energy for each sample. The mean gray level of each sample is obtained getting the mean of all gray levels of the tracks in the images of that sample. We adopted a similar process to obtain the mean diameters. Then, the results are related to the incident energy (Figure 10).

Sample	Manual counting ($\mu \pm \sigma$)		Automatic counting ($\mu \pm \sigma$)		Efficiency $\pm \sigma$	
	4.5 min	8.5 min	4.5 min	8.5 min	4.5 min	8.5 min
K0	18 \pm 3	16 \pm 2	17 \pm 2	15 \pm 3	0.95 \pm 0.09	0.96 \pm 0.15
K20	21 \pm 4	18 \pm 4	20 \pm 5	16 \pm 4	0.98 \pm 0.11	0.91 \pm 0.19
K30	19 \pm 4	19 \pm 4	19 \pm 5	17 \pm 5	0.99 \pm 0.10	0.92 \pm 0.14
K40	19 \pm 4	17 \pm 4	10 \pm 4	15 \pm 6	0.95 \pm 0.11	0.89 \pm 0.21
K50	21 \pm 2	17 \pm 3	20 \pm 3	15 \pm 4	0.94 \pm 0.09	0.89 \pm 0.15
K60	22 \pm 4	19 \pm 4	21 \pm 4	17 \pm 6	0.95 \pm 0.10	0.90 \pm 0.13
K70	18 \pm 4	14 \pm 3	17 \pm 4	12 \pm 4	0.96 \pm 0.10	0.88 \pm 0.15
K80	18 \pm 4	16 \pm 4	17 \pm 4	14 \pm 5	0.91 \pm 0.14	0.92 \pm 0.19
K90	20 \pm 4	17 \pm 3	19 \pm 5	18 \pm 5	0.96 \pm 0.14	1.01 \pm 0.22

Table 2: Mean, standard deviation, and automatic/manual efficiency ratio for for each sample of the first dataset, when ignoring border tracks.

When measuring track features such as gray levels or diameter products, the two scenarios studied here (considering or ignoring border tracks) lead to similar results (Figure 10). This is due to the subsequent choice of ROI according to their eccentricity, which ensures reliable track candidates in the two scenarios.

The diameter products roughly reflect the electronic energy loss (dE/dx) curve for ^{78}Kr in DAP (Figure 10 (a) and (c)), calculated with the software SRIM [32]. The Bragg peak appears around 100 MeV. Further scatter of points can be attributed to poor control of etching conditions. The uncertainty of 3 °C in temperature may cause a large variation in etching results [40]. Variations in gray level means are damped probably because this set was acquired in reflected illumination mode, which privileges surface details over depth effects.

3.2. Processing photomicrographs of fission tracks in DAP

In photomicrographs from dataset 1, our main concern was track superposition. However, all tracks were similar, created by a collimated beam of ^{78}Kr tracks. Here we go one step ahead, applying WUSEM to images where tracks present a variety of shapes. This image dataset was obtained from DAP plaques irradiated with thermal neutrons, coupled with apatite mounts. Fission fragments are born in the interior of the mineral, then emitted at different directions towards the detector. For instance, round tracks were created by perpendicular

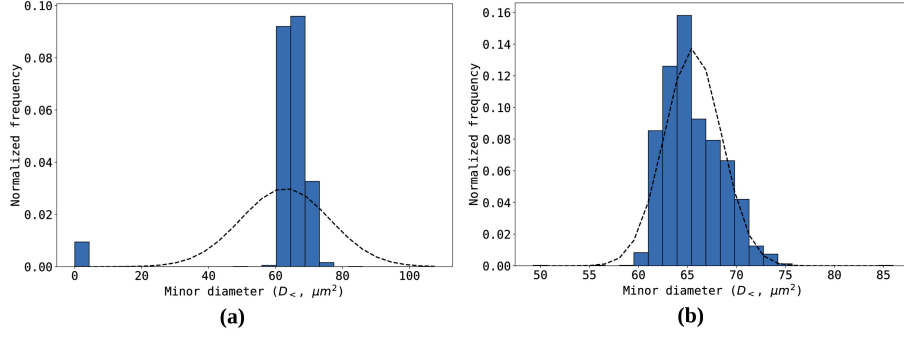


Figure 8: Histogram of minor diameters ($D_{<}$) of regions in the samples 4.5 min as separated by WUSEM algorithm, considering borders scenario. WUSEM seems to introduce small regions in the images, as seen in (a); we use only regions within the interval $\mu \pm 3\sigma$ to have reliable results. (a) histogram of all samples ($\mu = 62.887$, $\sigma = 13.329$). (b) histogram of samples within $\mu \pm 3\sigma$ ($\mu = 65.555$, $\sigma = 2.9062$). Dashed lines: normal probability density functions (PDF) fitted.

incident fragments, while the elliptical ones were created by particles hitting DAP surface at shallower angles (Figure 11).

As in the previous analysis, the manual counting performed by an experienced observer is taken as reference because we expect the observer to be able to recognize tracks efficiently. However, in this case, we do not expect the observer efficiency to 100 %. Fragments hitting the detector at lower energies originate tracks that are very difficult to distinguish from detector surfaces. An experienced observer would avoid counting those tracks to keep hers/his counting efficiency constant.

Repeating the previous processes for photomicrographs in dataset 2, we first binarize a test photomicrograph³ (Figure 11) using the ISODATA threshold. The binarized image is generated for two scenarios: considering and ignoring border tracks. Here, regions in the binary image are also filled using the function `ndimage.morphology.binary_fill_holes()` from `scipy`.

³Image “FT-Lab.19.07.390.MAG1.jpg”, from the folder `orig_figures/dataset.02`. Available in the Supplementary Material.

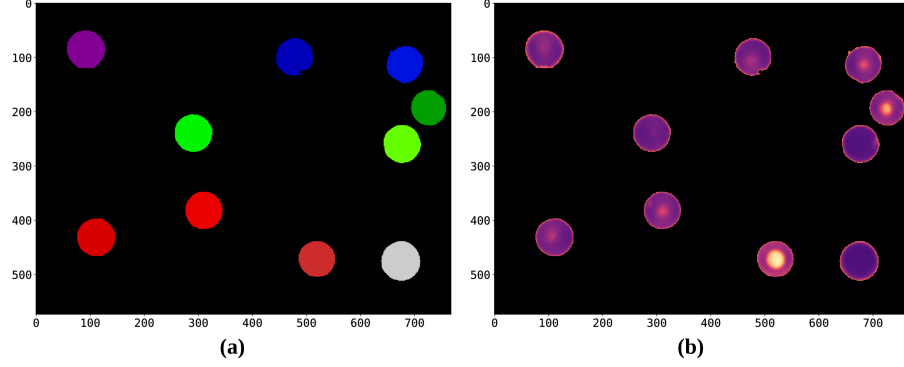


Figure 9: Regions from Figure 3 complying with $\epsilon \leq 0.3$. (a) labeled regions. (b) tracks correspondent to (a) in their original gray levels. Colormaps: (a) `nipy_spectral`. (b) `magma`.

Then we apply the WUSEM algorithm. We chose `initial_radius` = 5 and `delta_radius` = 2 as parameters, and the WUSEM result as parameter in the function `enumerate_objects()` (Figure 12).

For this dataset, we established an arbitrary tolerance of 10 tracks less than the mean of the manual counting. In this case, WUSEM's parameters become candidates if $0 < \mu_{n_{manual}} - n_{auto} < 10$, where n is the track number obtained by each approach. According to the stated comparison, the best parameters are `initial_radius` = 10 and `delta_radius` = 8 for both scenarios. This candidate presents the larger `initial_radius` and appears for both magnifications. Using the best parameters defined, we compared manual and automatic counting for each sample (Figure 13, Table 3).

WUSEM succeeded in avoiding false positives in this application (most samples are below the 1:1 line in Figures 13 (b, d)). Still, the user could apply more restrictive criteria. Also, it is worth noting the efficiency variation between the two image sets. Bigger objects are easier to be treated, thus automatic track counting in greater magnification images resulted in a higher counting efficiency (Table 3).

In this study, we used disks as structuring elements for processing images in both datasets. Since tracks in photomicrographs from dataset 1 are almost

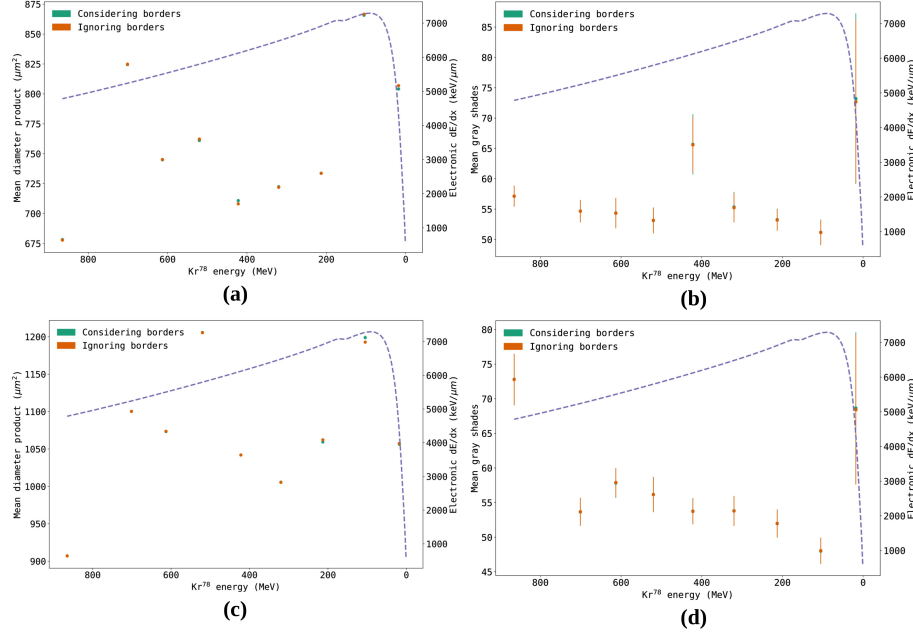


Figure 10: Relation between incident energy versus mean diameter product ((a) 4.5 min; (c) 8.5 min samples, left Y axis) and incident energy versus mean gray levels ((b) 4.5 min; (d) 8.5 min samples, left Y axis). Purple dashed line: electronic energy loss calculated with SRIM (right Y axis).

isotropic (as seen in Figure 3), disks are suitable structuring elements to be used in their segmentation. However, tracks within images in dataset 2 do not have a defined format (Figure 11). Employing different structuring elements, e.g. rotated cones or ellipses, could improve their segmentation and the automatic counting result.

3.3. False positives, false negatives and counting efficiency

In track counting, reproducibility is not about counting every track in the image, but counting the same types of tracks every time. It is the primary concern in FTD: for instance, the efficiencies for counting tracks in the standard sample should not vary when using zeta age calibrations [41, 42]. For absolute methods of determining neutron fluence [43], the efficiency should be constant when counting tracks in unknown age samples. The fast-growing areas of FTD

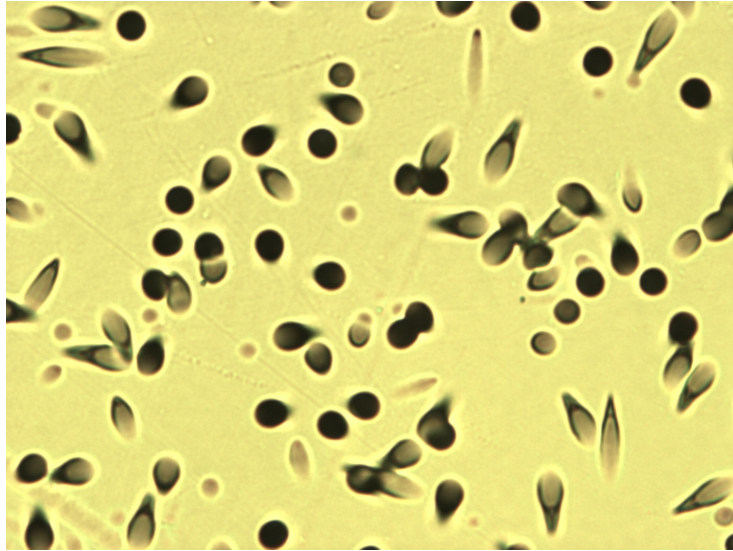


Figure 11: Input test photomicrograph from the second dataset, presenting tracks in a DAP sample. Colormap: `gray`.

using the Laser Ablation Inductively Couple Plasma Mass Spectrometer (LA-ICP-MS, [44, 45, 46, 47]) or the Electron Microprobe ([48, 49]) have the same efficiency issues, and could also benefit from automatic counting.

The major challenge for reproducibility is avoiding false positives, spurious objects such as scratches on the detector or mineral surface and other etching figures which automatic counting algorithms could misrepresent as tracks. In most situations, it is preferable to restrict the criteria, thus increasing the number of false negatives (not counted tracks), even implying in efficiency reduction.

Even more experienced observers expect some decreasing in efficiency due to superposition when counting tracks in high track density samples. This loss tends to be more severe in automatic counting. When applying algorithms as WUSEM, the separation of tracks in objects formed of several tracks is not always possible.

Counting less tracks than the actual number in a cluster is acceptable; however, when processing a large number of clusters in higher track density samples, we expect a lower efficiency when compared with lower track density samples.

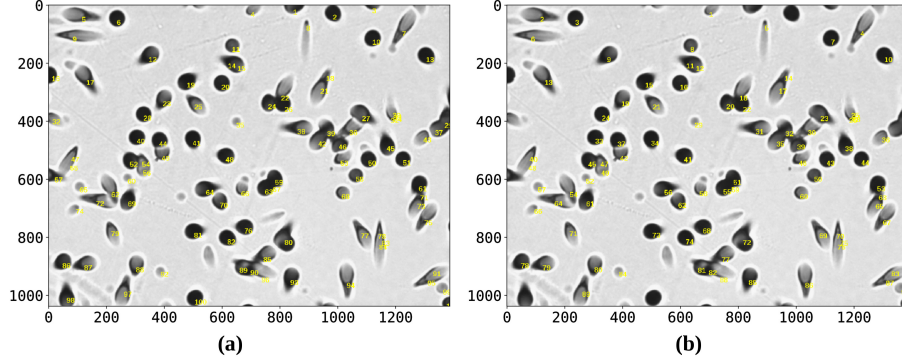


Figure 12: Tracks separated in Figure 11 using the WUSEM algorithm, and then enumerated using the function `enumerate_objects()`. As in Figure 5, the size of the first structuring element is small when compared to the objects, and smaller regions where tracks overlap are counted as tracks. (a) Considering border tracks. (b) Ignoring border tracks. Parameters for WUSEM algorithm: `initial_radius = 5`, `delta_radius = 2`.

This effect can be assessed by calibrating the efficiency as a function of track density. Therefore, efficiencies presented for WUSEM (Tables 1, 2 and 3) only hold for the track densities of the used samples.

4. Conclusion

In this paper we detect overlapping tracks in photomicrographs using WUSEM, an automatic segmentation algorithm based on image processing tools. WUSEM performs well in images containing overlapping circular tracks (from a ^{78}Kr collimated beam) and in photomicrographs with fission tracks at various orientations, both in DAP. The results are encouraging: the automatic/manual counting efficiency ratio is higher than 0.87 for all tested samples. We show also that diameter and eccentricity criteria increase the reliability of this method.

Since WUSEM using circles as structuring elements is aimed to tracks in DAP, which are isotropically etched, this technique is not suitable for separating tracks in mineral surfaces. Etching velocity in mineral surfaces depends on the crystal orientation, yielding more complex etching figures. Also, natural minerals are richer in scratches and other etching figures that can be mistaken

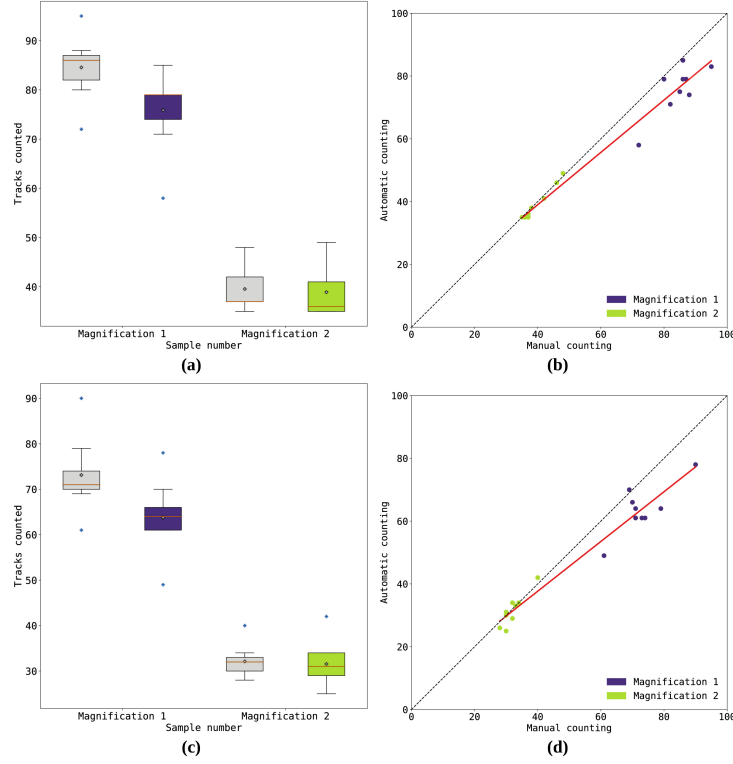


Figure 13: Comparison between manual and automatic counting for photomicrographs in the second dataset, when (a, b) considering border tracks and (c, d) ignoring border tracks. Automatic results are closer to manual ones when ignoring border tracks. (a, c) gray: manual counting. Red line: distribution median. White signal: distribution mean. Blue dots: outliers.

with fission tracks, especially when using image processing techniques. WUSEM could be studied to separate tracks in mineral surfaces; for that, it would need to use different structuring elements, which have to consider the orientation and shape of each track.

Acknowledgements

The authors would like to thank Matthias Schröter for his insights, and Christina Trautmann for the sample irradiation at GSI in Darmstadt. This work is supported by the São Paulo Research Foundation (FAPESP), grants #

Magnifi- cation	Counting border tracks			Ignoring border tracks		
	Manual counting ($\mu \pm \sigma$)	Automatic counting ($\mu \pm \sigma$)	Effi- ciency $\pm \sigma$	Manual counting ($\mu \pm \sigma$)	Automatic counting ($\mu \pm \sigma$)	Effi- ciency $\pm \sigma$
K0	24 ± 4	23 ± 3	22 ± 3	22 ± 3	0.93 ± 0.08	0.96 ± 0.09
K20	29 ± 5	27 ± 5	27 ± 5	25 ± 4	0.93 ± 0.11	0.95 ± 0.13
K30	27 ± 4	28 ± 4	26 ± 4	28 ± 6	0.95 ± 0.07	0.99 ± 0.10
K40	27 ± 4	27 ± 6	26 ± 3	26 ± 6	0.96 ± 0.10	0.98 ± 0.11
K50	28 ± 3	26 ± 5	26 ± 4	23 ± 4	0.94 ± 0.12	0.90 ± 0.09
K60	30 ± 4	28 ± 5	30 ± 5	27 ± 6	0.99 ± 0.07	0.96 ± 0.12
K70	23 ± 4	21 ± 5	22 ± 4	20 ± 6	0.97 ± 0.09	0.97 ± 0.11
K80	24 ± 4	24 ± 6	23 ± 4	23 ± 5	0.97 ± 0.09	0.98 ± 0.14
K90	28 ± 4	25 ± 4	29 ± 6	27 ± 6	1.02 ± 0.10	1.05 ± 0.12

Table 3: Mean, standard deviation, and automatic/manual efficiency ratio for for each sample of the first dataset, when considering border tracks.

2014/22922-0 and 2015/24582-4.

Supplementary material

The supplementary material for this study, including supplementary methods, results, code, and instructions is available at https://github.com/alexandrejaguar/publications/tree/master/2017/dap_segmentation.

References

References

- [1] G. A. Wagner, P. Van den Haute, Fission-Track Dating, Springer Netherlands, Dordrecht, 1992. doi:10.1007/978-94-011-2478-2.
URL <http://link.springer.com/10.1007/978-94-011-2478-2>
- [2] T. Tsuruta, Characteristics of diallyl phthalate resin as a fission track detector, Radiation Measurements 31 (1-6) (1999) 99-102. doi:10.1016/S1350-4487(99)00108-0.
URL <http://linkinghub.elsevier.com/retrieve/pii/S1350448799001080>

- [3] Y. Koguchi, T. Tsuruta, Polymerizing condition of DAP resin as fission track detector, *Radiation Measurements* 35 (3) (2002) 171–175. doi:10.1016/S1350-4487(02)00044-6.
URL <http://linkinghub.elsevier.com/retrieve/pii/S1350448702000446>
- [4] T. Yoshioka, T. Tsuruta, H. Iwano, T. Danhara, Y. Koguchi, Fission-fragment registration and etching properties of diallyl phthalate with reference to its use as an external detector in fission-track dating, *Nuclear Instruments and Methods in Physics Research Section B: Beam Interactions with Materials and Atoms* 207 (3) (2003) 323–332. doi:10.1016/S0168-583X(03)00508-1.
URL <http://linkinghub.elsevier.com/retrieve/pii/S0168583X03005081>
- [5] T. Danhara, H. Iwano, T. Yoshioka, T. Tsuruta, Zeta calibration values for fission track dating with a diallyl phthalate detector, *The Journal of the Geological Society of Japan* 109 (11) (2003) 665–668. doi:10.5575/geosoc.109.665.
URL https://www.jstage.jst.go.jp/article/geosoc1893/109/11/109_11_665/_article
- [6] K. Moriwaki, Y. Shimpuku, M. Makimura, Improvement of Track Counting Accuracy and Efficiency in the Fission Track Method., *Radioisotopes* 47 (8) (1998) 611–616. doi:10.3769/radioisotopes.47.611.
URL https://www.jstage.jst.go.jp/article/radioisotopes1952/47/8/47_8_611/_article
- [7] A. J. W. Gleadow, S. J. Gleadow, D. X. Belton, B. P. Kohn, M. S. Krochmal, R. W. Brown, Coincidence mapping - a key strategy for the automatic counting of fission tracks in natural minerals, *Geological Society, London, Special Publications* 324 (1) (2009) 25–36. doi:10.1144/SP324.2.
URL <http://sp.lyellcollection.org/lookup/doi/10.1144/SP324.2>

- [8] R. C. Gonzalez, R. E. Woods, Digital Image Processing, 3rd Edition, Pearson, Upper Saddle River, NJ, USA, 2007.
- [9] D. Azimi-Garakani, J. G. Williams, Automatic fission track counting using the Quantimet 720, Nuclear Instruments and Methods 147 (1977) 69–73.
- [10] J. Beer, J. Pipper, W. Heinrich, Automatic measurements of nuclear tracks in plastic foils, Journal of Physics E: Scientific Instruments 15 (4) (1982) 439–443.
URL <http://stacks.iop.org/0022-3735/15/i=4/a=013>
- [11] P. B. Price, W. Krischer, Semi-automated, three-dimensional measurement of etched tracks in solid-state nuclear track detectors, Nuclear Instruments and Methods in Physics Research Section A: Accelerators, Spectrometers, Detectors and Associated Equipment 234 (1) (1985) 158–167.
- [12] W. Trakowski, B. Schöfer, J. Dreute, S. Sonntag, C. Brechtmann, J. Beer, H. Drechsel, W. Heinrich, An automatic measuring system for particle tracks in plastic detectors, Nuclear Instruments and Methods in Physics Research 225 (1) (1984) 92–100. doi:10.1016/0167-5087(84)91342-5.
- [13] S. Masumoto, K. Wadatsumi, Computerized Image-Processing System for Fission-Track Dating, Geoinformatics 1 (1) (1990) 93–102.
- [14] K. Wadatsumi, S. Masumoto, Three-dimensional measurement of fission-tracks: Principles and an example in zircon from the Fish Canyon tuff, International Journal of Radiation Applications and Instrumentation. Part D. Nuclear Tracks and Radiation Measurements 17 (3) (1990) 399–406. doi:10.1016/1359-0189(90)90063-4.
URL <http://linkinghub.elsevier.com/retrieve/pii/1359018990900634>
- [15] A. P. Fews, Fully automated image analysis of etched tracks in CR-39, Nuclear Instruments and Methods in Physics Research Section B: Beam Interactions with Materials and Atoms 71 (4) (1992) 465–478.

doi:10.1016/0168-583X(92)95367-Z.

URL <http://linkinghub.elsevier.com/retrieve/pii/S0168583X9295367Z>

- [16] N. Petford, J. A. Miller, Three-dimensional imaging of fission tracks using confocal scanning laser microscopy, *American Mineralogist* 77 (1992) 529–533.
- [17] N. Petford, J. A. Miller, J. Briggs, The automated counting of fission tracks in an external detector by image analysis, *Computers & Geosciences* 19 (4) (1993) 585–591. doi:10.1016/0098-3004(93)90084-I.
URL <http://linkinghub.elsevier.com/retrieve/pii/S009830049390084I>
- [18] G. Espinosa, R. B. Gammage, K. E. Meyer, C. S. Dudney, Nuclear track analysis by digital imaging, *Radiation Protection Dosimetry* 66 (1-4) (1996) 363–366.
- [19] A. Boukhair, A. Haessler, J. C. Adlo, A. Nourreddine, New code for digital imaging system for track measurements, *Nuclear Instruments and Methods in Physics Research. Section B, Beam Interactions with Materials and Atoms* 160 (2000) 550–555.
- [20] M. Dolleiser, S. R. Hashemi-Nezhad, A fully automated optical microscope for analysis of particle tracks in solids, *Nuclear Instruments and Methods in Physics Research, Section B: Beam Interactions with Materials and Atoms* 198 (1-2) (2002) 98–107. doi:10.1016/S0168-583X(02)01484-2.
- [21] R. Bedogni, Development of a reader for the routine analysis of CR-39 fast neutron dosimeters: improvement of the dosimetric performance using automatic vision and motion tools, *Radiation Measurements* 36 (1-6) (2003) 239–243. doi:10.1016/S1350-4487(03)00131-8.
URL <http://linkinghub.elsevier.com/retrieve/pii/S1350448703001318>

- [22] N. Yasuda, K. Namiki, Y. Honma, Y. Umeshima, Y. Marumo, H. Ishii, E. R. Benton, Development of a high speed imaging microscope and new software for nuclear track detector analysis, *Radiation Measurements* 40 (2-6) (2005) 311–315. doi:10.1016/j.radmeas.2005.02.013.
- [23] H. Tawara, K. Eda, K. Takahashi, T. Doke, N. Hasebe, S. Kodaira, S. Ota, M. Kurano, N. Yasuda, Development of an automated multisample scanning system for nuclear track etched detectors, *Nuclear Instruments and Methods in Physics Research, Section A: Accelerators, Spectrometers, Detectors and Associated Equipment* 593 (3) (2008) 475–480. doi:10.1016/j.nima.2008.05.035.
- [24] A. F. de Siqueira, W. M. Nakasuga, A. Pagamisse, C. A. Tello Saenz, A. E. Job, An automatic method for segmentation of fission tracks in epidote crystal photomicrographs, *Computers and Geosciences* 69 (2014) 55–61. doi:10.1016/j.cageo.2014.04.008.
URL <http://dx.doi.org/10.1016/j.cageo.2014.04.008>
- [25] J. Ruan, H. Li, J. Zhang, Z. Zhang, L. Chen, J. Song, J. Liu, J. Liu, Image mosaic method for recognition of proton track in nuclear emulsions, *Nuclear Instruments and Methods in Physics Research Section A: Accelerators, Spectrometers, Detectors and Associated Equipment* 762 (2014) 16–21. doi:10.1016/j.nima.2014.05.040.
URL <http://dx.doi.org/10.1016/j.nima.2014.05.040><http://linkinghub.elsevier.com/retrieve/pii/S0168900214005671>
- [26] E. Enkelmann, T. A. Ehlers, G. Buck, A. K. Schatz, Advantages and challenges of automated apatite fission track counting, *Chemical Geology* 322–323 (2012) 278–289. doi:10.1016/j.chemgeo.2012.07.013.
URL <http://dx.doi.org/10.1016/j.chemgeo.2012.07.013>
- [27] S. Beucher, C. Lantuejoul, Use of Watersheds in Contour Detection (1979). doi:citeulike-article-id:4083187.
URL <http://www.citeulike.org/group/7252/article/4083187>

- [28] J. Serra, Image analysis and mathematical morphology, Vol. 1, Academic press, 1982.
- [29] F. M. Schaller, M. Neudecker, M. Saadatfar, G. Delaney, K. Mecke, G. E. Schröder-Turk, M. Schröter, Tomographic analysis of jammed ellipsoid packings, in: AIP Conference Proceedings, Vol. 1542, 2013, pp. 377–380. doi:10.1063/1.4811946.
URL <http://aip.scitation.org/doi/abs/10.1063/1.4811946>
- [30] B. Smilgys, S. Guedes, M. Morales, F. Alvarez, J. C. Hadler, P. R. P. Coelho, P. T. D. Siqueira, I. Alencar, C. J. Soares, E. A. C. Curvo, Boron thin films and CR-39 detectors in BNCT: A method to measure the $^{10}\text{B}(n,\alpha)^7\text{Li}$ reaction rate, Radiation Measurements 50 (2013) 181–186. doi:10.1016/j.radmeas.2012.07.001.
URL <http://dx.doi.org/10.1016/j.radmeas.2012.07.001>
- [31] C. Fiorio, J. Gustedt, Two linear time Union-Find strategies for image processing, Theoretical Computer Science 154 (2) (1996) 165–181. doi:10.1016/0304-3975(94)00262-2.
- [32] J. F. Ziegler, M. D. Ziegler, J. P. Biersack, SRIM - The stopping and range of ions in matter (2010), Nuclear Instruments and Methods in Physics Research, Section B: Beam Interactions with Materials and Atoms 268 (11-12) (2010) 1818–1823. doi:10.1016/j.nimb.2010.02.091.
URL <http://dx.doi.org/10.1016/j.nimb.2010.02.091>
- [33] S. van der Walt, S. C. Colbert, G. Varoquaux, The NumPy Array: A Structure for Efficient Numerical Computation, Computing in Science & Engineering 13 (2) (2011) 22–30. doi:10.1109/MCSE.2011.37.
URL <http://ieeexplore.ieee.org/document/5725236/>
- [34] E. Jones, T. Oliphant, P. Peterson, SciPy: Open source scientific tools for Python (2001–).
URL <http://www.scipy.org/>

- [35] J. D. Hunter, Matplotlib: A 2D Graphics Environment, Computing in Science & Engineering 9 (3) (2007) 90–95. doi:10.1109/MCSE.2007.55.
URL <http://ieeexplore.ieee.org/document/4160265/>
- [36] S. van der Walt, J. L. Schönberger, J. Nunez-Iglesias, F. Boulogne, J. D. Warner, N. Yager, E. Gouillart, T. Yu, scikit-image: image processing in Python, PeerJ 2 (2014) e453. arXiv:1407.6245, doi:10.7717/peerj.453.
URL <https://peerj.com/articles/453>
- [37] G. van Rossum, Python Reference Manual, Tech. rep., Centrum voor Wiskunde en Informatica (CWI), Amsterdam (1995).
URL <https://ir.cwi.nl/pub/5008/05008D.pdf>
- [38] G. H. Ball, D. J. Hall, A clustering technique for summarizing multivariate data, Behavioral Science 12 (2) (1967) 153–155. doi:10.1002/bs.3830120210.
- [39] T. W. Ridler, S. Calvard, Picture Thresholding Using an Iterative Selection Method, IEEE Transactions on Systems, Man and Cybernetics 8 (8) (1978) 630–632. doi:10.1109/TSMC.1978.4310039.
- [40] S. Guedes, J. C. Hadler, P. J. Iunes, S. R. Paulo, C. A. Tello, On the reproducibility of SSNTD track counting efficiency, Nuclear Instruments and Methods in Physics Research Section A: Accelerators, Spectrometers, Detectors and Associated Equipment 418 (2-3) (1998) 429–433. doi:10.1016/S0168-9002(98)00918-8.
URL <http://linkinghub.elsevier.com/retrieve/pii/S0168900298009188>
- [41] A. J. Hurford, P. F. Green, The zeta age calibration of fission-track dating, Chemical Geology 41 (1983) 285–317. doi:10.1016/S0009-2541(83)80026-6.
URL <http://linkinghub.elsevier.com/retrieve/pii/S0009254183800266>

- [42] A. J. Hurford, Standardization of fission track dating calibration: Recommendation by the Fission Track Working Group of the I.U.G.S. Subcommittee on Geochronology, *Chemical Geology: Isotope Geoscience Section* 80 (2) (1990) 171–178. doi:10.1016/0168-9622(90)90025-8.
- [43] C. J. Soares, I. Alencar, S. Guedes, R. H. Takizawa, B. Smilgys, J. C. Hadler, Alpha spectrometry study on LR 115 and Makrofol through measurements of track diameter, *Radiation Measurements* 50 (2013) 246–248. doi:10.1016/j.radmeas.2012.06.010.
- [44] J. C. Hadler, P. J. Iunes, C. A. Tello, F. Chemale, K. Kawashita, E. A. C. Curvo, F. G. S. Santos, T. E. Gasparini, P. A. F. P. Moreira, S. Guedes, Experimental study of a methodology for Fission-track Dating without neutron irradiation, *Radiation Measurements* 44 (9-10) (2009) 955–957. doi:10.1016/j.radmeas.2009.10.081.
URL <http://dx.doi.org/10.1016/j.radmeas.2009.10.081><http://linkinghub.elsevier.com/retrieve/pii/S1350448709002571>
- [45] N. Hasebe, J. Barbarand, K. Jarvis, A. Carter, A. J. Hurford, Apatite fission-track chronometry using laser ablation ICP-MS, *Chemical Geology* 207 (3-4) (2004) 135–145. doi:10.1016/j.chemgeo.2004.01.007.
- [46] C. J. Soares, S. Guedes, J. C. Hadler, R. Mertz-Kraus, T. Zack, P. J. Iunes, Novel calibration for LA-ICP-MS-based fission-track thermochronology, *Physics and Chemistry of Minerals* 41 (1) (2014) 65–73. doi:10.1007/s00269-013-0624-2.
- [47] C. J. Soares, R. Mertz-Kraus, S. Guedes, D. F. Stockli, T. Zack, Characterisation of Apatites as Potential Uranium Reference Materials for Fission-track Dating by LA-ICP-MS, *Geostandards and Geoanalytical Research* 39 (3) (2015) 305–313. doi:10.1111/j.1751-908X.2014.00301.x.
URL <http://doi.wiley.com/10.1111/j.1751-908X.2014.00301.x>
- [48] D. J. Gombosi, J. I. Garver, S. L. Baldwin, On the development of electron microprobe zircon fission-track geochronology, *Chemical Geology* 363

(2014) 312–321. doi:10.1016/j.chemgeo.2013.11.005.

URL <http://dx.doi.org/10.1016/j.chemgeo.2013.11.005>

- [49] A. N. C. Dias, F. Chemale, C. J. Soares, S. Guedes, A new approach for electron microprobe zircon fission track thermochronology, *Chemical Geology* 459 (January) (2017) 129–136. doi:10.1016/j.chemgeo.2017.04.014.

URL <http://dx.doi.org/10.1016/j.chemgeo.2017.04.014>